Solution structure of Apaf-1 CARD and its interaction with caspase-9 CARD: A structural basis for specific adaptor/caspase interaction

Pei Zhou*, James Chou*, Roberto Sanchez Olea†, Junying Yuan†, and Gerhard Wagner*‡

*Department of Biological Chemistry and Molecular Pharmacology, Harvard Medical School, Boston, MA 02115; and †Department of Cell Biology, Harvard Medical School, Boston, MA 02115

ABSTRACT   Direct recruitment and activation of caspase-9 by Apaf-1 through the homophilic CARD/CARD (*Ca*spase *R*ecruitment *Do*main) interaction is critical for the activation of caspases downstream of mitochondrial damage in apoptosis. Here we report the solution structure of the Apaf-1 CARD domain and its surface of interaction with caspase-9 CARD. Apaf-1 CARD consists of six tightly packed amphipathic α-helices and is topologically similar to the RAIDD CARD, with the exception of a kink observed in the middle of the N-terminal helix. By using chemical shift perturbation data, the homophilic interaction was mapped to the acidic surface of Apaf-1 CARD centered around helices 2 and 3. Interestingly, a significant portion of the chemically perturbed residues are hydrophobic, indicating that in addition to the electrostatic interactions predicted previously, hydrophobic interaction is also an important driving force underlying the CARD/CARD interaction. On the basis of the identified functional residues of Apaf-1 CARD and the surface charge complementarity, we propose a model of CARD/CARD interaction between Apaf-1 and caspase-9.

Apoptosis plays an essential role in cell development, tissue homeostasis, and defense against pathogens. Failure of cells to undergo apoptosis can lead to cancer or autoimmune disease, whereas excessive apoptosis may be involved in AIDS and neurodegenerative disease (1). Apoptosis is intricately regulated through multiple signaling pathways (2–4). The death signals originating from death receptors, such as Fas or tumor necrosis factor receptors, are transduced through the recruitment of procaspase-8 to the death-induced signaling complex by the adapter molecule FADD/MORT1 (5, 6). The local aggregation of procaspase-8 is sufficient to allow auto- or transprocessing to produce active caspase-8, which can subsequently activate downstream executioners, such as caspases 3, 6 and 7 (2, 6, 7). Cell-death signals can also be initiated after the release of cytochrome *c* resulting from mitochondrial damage. This pathway requires the function of Apaf-1, the human homologue of *Caenorhabditis elegans* cell-death gene product (CED-4), which is responsible for the recruitment of procaspase-9. In the presence of dATP and cytochrome *c*, the 1:1 complex of Apaf-1 and procaspase-9 is able to activate caspase-9 (8, 9), which leads to subsequent activation of downstream caspases (10). The essential roles of Apaf-1 and caspase-9 have been confirmed by knockout experiments in mice (11–14). Mice lacking the Apaf-1 gene or caspase-9 gene show an excessive number of neurons in their brains and defects in facial features, because of a defect in apoptosis. In addition, Apaf-1/caspase-9 interaction is shown to be an essential component of p53-regulated apoptosis (15). Re-

cently, crosstalk between the two pathways has been established through caspase-8 activation of BID (*B*H3 *I*nteracting Domain *D*eath agonist) (16, 17), indicating that apoptotic signals originating from Fas/tumor necrosis factor receptor 1 can be amplified by the mitochondrial pathway. Consistent with this finding, the ability of caspase-8 to activate downstream caspases was shown to depend on the presence of mitochondria in cell-free *Xenopus* egg extracts (18). In egg extracts devoid of the mitochondria, a significantly higher level of caspase-8 was required to activate downstream caspases, whereas in the presence of mitochondria, the effective activation of downstream caspases from low concentration of caspase-8 are vastly amplified after the release of cytochrome *c*.

The formation of Apaf-1/caspase-9 complex is accomplished by the CARD/CARD (*Ca*spase *R*ecruitment *Do*main) interaction, an apical step in the mitochondrial pathway. Additionally, homophilic CARD/CARD interactions are also found in an array of other proteins involved in apoptotic regulation, including a majority of the initiator procaspases, adapter proteins, and cellular apoptosis inhibitors (19). Importantly, extensive *in vitro* binding assays reveal that those homophilic interactions are highly specific, because Apaf-1 CARD interacts only with caspase-9 CARD, but not with other CARD-containing caspases. To understand the molecular basis underlying the specificity of the CARD/CARD interaction between caspase-9 and Apaf-1, the structural details of the interaction must be investigated.

In this study, we have determined the solution structure of Apaf-1 CARD using NMR spectroscopy. The structure reveals a six-helix bundle resembling the FADD DED (20), RAIDD CARD (21), and Fas DD (22). We have performed NMR experiments that monitor the chemical perturbations of Apaf-1 CARD while being titrated with caspase-9 CARD. On the basis of the titration data, the interaction surface of Apaf-1 CARD is identified. A model of homophilic interaction is derived from the perturbation data and the distinct charged patches observed on the surface of Apaf-1 and caspase-9 CARD. In relating our current results to the previous studies on the interaction domains including RAIDD and caspase-2 CARD, FADD DED, and Fas DD (20–23), the general mode of homophilic interaction is elucidated.

MATERIALS AND METHODS

Overexpression and Purification of Apaf-1 CARD (1–97) and Caspase-9 CARD (1–138). The CARD of human Apaf-1

1–97 was cloned into pGEX-2T vector. Apaf-1 CARD was expressed in *Escherichia coli* with glutathione *S*-transferase (GST) fused at the N terminus. The transformed cells were grown at 37°C and induced with 1 mM isopropyl-D-thiogalactoside in either LB medium (for unlabeled protein) or M9-minimal medium substituted with ^{15}N-NH$_4$Cl (1 g/L) for ^{15}N-labeled protein and ^{13}C-glucose (2 g/L) for uniform ^{13}C labeling. A 85% deuterated uniform ^{15}N, ^{13}C-labeled protein was prepared by growing the cells in 85% D$_2$O supplemented with ^{15}N-NH$_4$Cl and ^{13}C-glucose. Lysine-selective labeling was obtained by growing cells in M9 medium with 100 mg/L ^{15}N-labeled lysine. Ten percent ^{13}C labeled sample was obtained by using M9 medium (containing 2 g/L glucose) with 0.2 g/L ^{13}C-glucose.

After cell lysis, the GST-fused recombinant protein was purified by using GST affinity chromatography according to standard protocol. The N-terminal GST fusion protein was removed by thrombin cleavage and separated from Apaf-1 by using glutathione resin. The eluted Apaf-1 CARD was further purified to homogeneity by using gel filtration (Sephadex G-50, Amersham Pharmacia) and then exchanged into NMR buffer containing 20 mM phosphate (pH 6.5) and 50 mM NaCl in H$_2$O/D$_2$O (9/1) or D$_2$O.

Caspase-9 CARD (1–138) was cloned into pGEX-6P2 vector and purified in a similar way as described above except the transformed cells were induced at 15°C with 0.1 mM isopropyl-D-thiogalactoside overnight, and the fusion protein was cleaved at 4°C for 2 hr by using PreScission protease (Amersham Pharmacia). Purified caspase-9 CARD was exchanged into NMR buffer before titration.

NMR Spectroscopy. All NMR spectra were acquired at 27°C on Bruker 500 (Billerica, MA), Bruker 600, or Varian Inova 750 spectrometers. Sequential assignments were achieved by using two pairs of triple-resonance experiments [HNCA, HN-(CO)CA and HN(CA)CB, HN(COCA)CB] with uniformly ^{15}N, ^{13}C labeled, and 85% deuterated protein in 90% H$_2$O/10% D$_2$O (24, 25). In addition, amino acid-selective ^{15}N labeling of Lys was used to confirm the sequential assignment of amide protons. Side-chain proton resonances were mostly assigned by using three-dimensional Cbd-HCCH-total correlation spectroscopy (TOCSY) (26) and three-dimensional ^{15}N-dispersed TOCSY-heteronuclear sequential quantum correlation (HSQC) spectra, recorded by using uniformly ^{13}C-labeled protein in D$_2$O and uniformly ^{15}N-labeled protein in H$_2$O, respectively. The assignment of aromatic side chains was accomplished by using homonuclear TOCSY and nuclear Overhauser effect (NOE) spectroscopy experiments, acquired with the nonlabeled protein in D$_2$O. Stereospecific assignment of methyl groups of Val and Leu residues was obtained from ^{13}C-HSQC spectrum of a 10% ^{13}C-labeled protein (27). $^3J_{\text{HN-HA}}$ coupling was obtained through an heteronuclear multiple quantum correlation *J* experiment (28).

NMR Titration of Apaf-1 CARD and Caspase-9 CARD. Both Apaf-1 CARD (1–97) and caspase-9 CARD (1–138) were exchanged into NMR buffer before titration. A series of ^{1}H-^{15}N HSQC spectra were recorded by adding different amounts of nonlabeled caspase-9 CARD into ^{15}N-labeled Apaf-1 CARD. NMR samples were equilibrated at room temperature for at least 30 min before recording the NMR spectra.

Structural Calculation. Interproton distance constraints were derived from NOE spectroscopy crosspeak volumes, which were autocalibrated by using the CALIBA module included in the DYANA package (29). Dihedral angle constraints were generated by using HABAS based on $^3J_{\text{HN-HA}}$ couplings, the chemical shift index (30), and NOE patterns. Initial structures were generated by using the program DYANA starting from random conformations and refined by using simulated annealing protocol in X-PLOR (31). Loose hydrogen bond constraints were introduced at the late stage of structural

calculations and based on the characteristic NOE patterns observed for α-helix conformation. Of the 30 calculated structures, the 15 best with no NOE violation >0.4 Å and no dihedral angle violations >5.0 were presented in Fig. 1*A* and were used to generate the statistics (Table 1). These coordinates have been deposited with the Protein Data Bank (PDB ID codes 1C15 and RCSB009364).

RESULTS AND DISCUSSION

Structure Comparison Between Apaf-1 CARD and RAIDD CARD. Apaf-1 CARD consists of six closely packed antiparallel amphipathic α-helices arranged in a fold similar to that of RAIDD CARD. In both proteins, all helices are tightly packed against a hydrophobic core consisting of conserved residues in
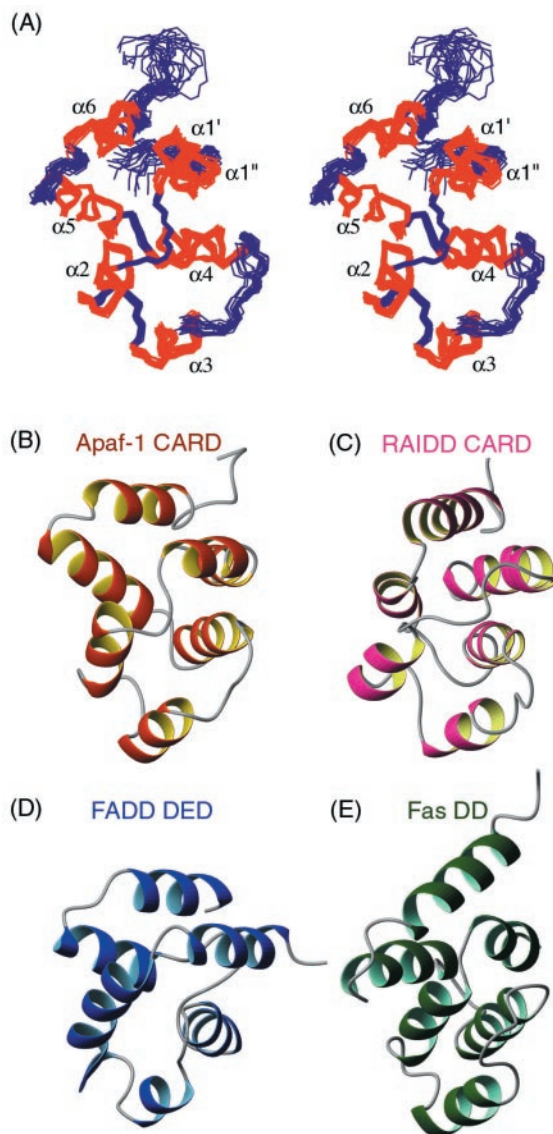

FIG. 1. Solution structure of Apaf-1 CARD resembles other homophilic interacting motifs in apoptosis. (*A*) Stereoview of the backbone atoms (N, C$^\alpha$, C′) of the 15 superimposed NMR-derived structures of Apaf-1 CARD. The helices are numbered α1–α6 accordingly. (*B–E*) Ribbon diagrams of Apaf-1 CARD shown in red (*B*), RAIDD CARD in pink (*C*), FADD DED in dark blue (*D*), and Fas DD in green (*E*), illustrating the conserved six-helix bundle motif as well as variations of helix orientations among different domains. The coordinates of RAIDD CARD, FADD DED, and Fas DD were obtained from the Protein Data Bank (accession codes 3crd, 1a1w, and 1ddf).

Biophysics: Zhou *et al.*

Proc. Natl. Acad. Sci. USA 96 (1999)   11267

Table 1. Structural statistics for the Apaf-1 CARD

NOE distance restraints	
All	1,219
Intraresidue	645
Sequential ($|i - j| = 1$)	214
Medium range ($|i - j| \leq 4$)	166
$i, i + 2$	9
$i, i + 3$	115
$i, i + 4$	32
Long range ($|i - j| \geq 5$)	118
H bonds*	76
Dihedral angle constraints†	322
Ramachandran plot‡	
Most favorable region, %	85.8
Additionally allows region, %	14.2
Generously allowed region, %	0.0
Disallowed region, %	0.0
Average RMS deviation to the mean structure	
Backbone (residues 3–91) Å	0.39
Heavy atoms (residues 3–91), Å	0.77

None of these structures exhibit distance violations greater than 0.4 Å or dihedral angle violations greater than 5°.

*Hydrogen bond for α-helices was added only at the late stage of structural calculations for residues with characteristic HN(i)-Hα ($i - 3, i - 4$) NOEs observed in the three-dimensional ^{15}N-NOE spectroscopy-HSQC spectrum.

†Dihedral angle constraints were generated by DYANA (29), based on $^3J_{HNH\alpha}$ couplings, Cα chemical shifts (30), and NOE constraints.

‡PROCHECK_NMR (35) was used to assess the quality of the structures.

the CARD family. However, there are significant differences between the two. In RAIDD CARD, the N-terminal helix is relatively straight, whereas in Apaf-1 CARD there exists a kink of 50° in the middle of α1 that subsequently disrupts it into two smaller helices, α1′ and α1″. The observed difference in the conformation of the N-terminal helix is caused by the different packing of helices in RAIDD and in Apaf-1 CARD. In RAIDD CARD, all helices (α1-α6) are roughly parallel to each other and can be divided into two groups. Helices 6, 5, and 2 reside on one side, packing against helices 1, 4, and 3 on the other side (Fig. 1*C*). In Apaf-1 CARD, only α2, α3, and α4 are parallel to each other, forming a characteristic three-helix bundle. The packing of α2, α3, and α4 is more compact in Apaf-1, which brings α2 closer to α3 compared with that of RAIDD CARD. Helix 5 (α5) is connected to α4 by a tight turn and crosses the surface of α2 and α4 at an angle of approximately 50°. Helix 6 (α6) pairs with α5 and lies in the same plane as α5. There thus exists a 50° angle between α6 and α4. The only solution to accommodate the different orientations and seal the gap between α6 and α4 is to disrupt helix 1 in Apaf-1 into two smaller helices so that α1′ (N-terminal to the kink) pairs with α4 and α1″ (C-terminal to the kink) pairs with α6 (Fig. 1 *A* and *B*). These structural variations of helical arrangements observed between Apaf-1 and RAIDD CARD most likely reflect sequence variations among different family members. For instance, the α4–α5 loop in Apaf-1 CARD is significantly shorter than that in RAIDD CARD, which might result in the different orientations of α4. Interestingly, the overall orientations of helices in Apaf-1 CARD are more similar to that of FADD DED (20). Among the six helices, α2, α3, and α5 have the most conserved orientations in Apaf-1 CARD, RAIDD CARD, and FAS DD (Fig. 1 *B–E*). These structural differences may contribute to the stringent selectivity of the homophilic interactions observed in the three families of interaction domains.

Apaf-1 CARD Interacts with Caspase-9 CARD Through the α2 and α3. In our previous studies of RAIDD CARD, we have observed a distinct polarity of the surface charge distribution (21). A similar dipolar surface charge distribution is also observed in the previously modeled CARD domains of

caspase-2, Apaf-1, and caspase-9. To identify the binding surface of Apaf-1, we performed titration experiments by recording ^{1}H-^{15}N HSQC spectra of ^{15}N-labeled Apaf-1 CARD while adding various amounts of the nonlabeled caspase-9 CARD. During the process, the ^{1}H-^{15}N resonances of K21, M26, D27, I30, S31, I37, S38, E41, N45, F71, Y72, A74, and L75 are progressively broadened because of the intermediate exchange rate of Apaf-1 CARD between the free and the complex states. Additionally, the ^{1}H-^{15}N resonances of I20, I25, M29, D32, F34, L35, T36, E39, E40, K42, V43, E46, S67, H77, E78, Y80, D82, and L83 are not severely broadened, but perturbed to various extents (Fig. 2*A*). The chemically perturbed residues in Apaf-1 CARD are clustered mainly around the acidic surface of Apaf-1 CARD. More specifically, they form a contiguous surface containing residues on α2 and α3, the α2–α3 loop, the C terminus of α5, and the α5–α6 loop. The central acidic region consists of D27, D32, and E40, which are flanked by E41, E46, D64, D66, E78, and D82 (Fig. 2*B*). Surprisingly, a significant number of the chemically perturbed residues are hydrophobic. The largest surface-exposed hydrophobic patch, formed by I20, Y24, I25, and Y80, is located between the α2, the terminus of α5, and the α5–α6 loop. Several other surface-exposed hydrophobic residues, such as L35 (α2–α3 loop), I37 (α3), V43 (α3), Y72 (α5), and L76 (α5), are also affected during the titration. All the chemically perturbed residues except F71 are more or less surface exposed and thus can readily participate in the CARD/CARD interaction. F71, located in the middle of α5, is completely buried in the hydrophobic core formed by hydrophobic residues of α1, α2, α5, and α6. Because F71 is unlikely to be directly involved in interacting with caspase-9 CARD in its buried state, the detected chemical-shift perturbation of F71 thus suggests that, during the assembly of CARD/CARD complex, the position of α5 may be altered. This reorientation of α5 would possibly expose the previously inaccessible hydrophobic patch consisting of F71, Y72, A74, and L75, and thereby enables it to readily interact with caspase-9 (Fig. 3*A*). On the other hand, Y24, which resides in the hydrophobic patch surrounded by other surface exposed and chemically perturbed residues such as I20, I25, and Y80, does not show chemical shift perturbation on caspase-9 binding. Although all residues showing chemical shift perturbations must be located on the protein interacting surface, not all the interacting residues exhibit significant chemical shift perturbations. A good example of this has been shown by Sun *et al.* (32). Thus, one would need to consider the overall distribution of chemically perturbed residues to map the correct interaction surface. Because of the fact that Y24 is a major component of the hydrophobic cluster containing also I20, I25, and Y80, and because residues I20, I25, and Y80 all display chemical perturbations on caspase-9 binding, it is very likely that Y24 also participates in the Apaf-1/caspase-9 interaction.

The mechanism of caspase-9 activation remains a matter of debate. A recent study suggests the involvement of Apaf-1 oligomerization before the processing of procaspase-9 (9). The NMR spectra of Apaf-1 CARD alone and in complex with caspase-9 CARD indicate that neither of them exists in oligomeric state at NMR concentration ($\approx$1 mM). Therefore, it is unlikely that CARD participates in Apaf-1 oligomerization.

Comparisons of Different Homophilic Interactions. Because of its nature as an interaction motif, Apaf-1 CARD, a member of the prominent CARD family, is likely to share some common functional elements with other CARDs, as well as the death recruitment domains outside the CARD family, such as DD and DED. Hence, comparing the different homophilic interactions can potentially lead to insightful observations. To summarize the titration data presented in the previous section, the binding surface of Apaf-1 CARD (primarily acidic) encompasses α2 and α3, while being partially

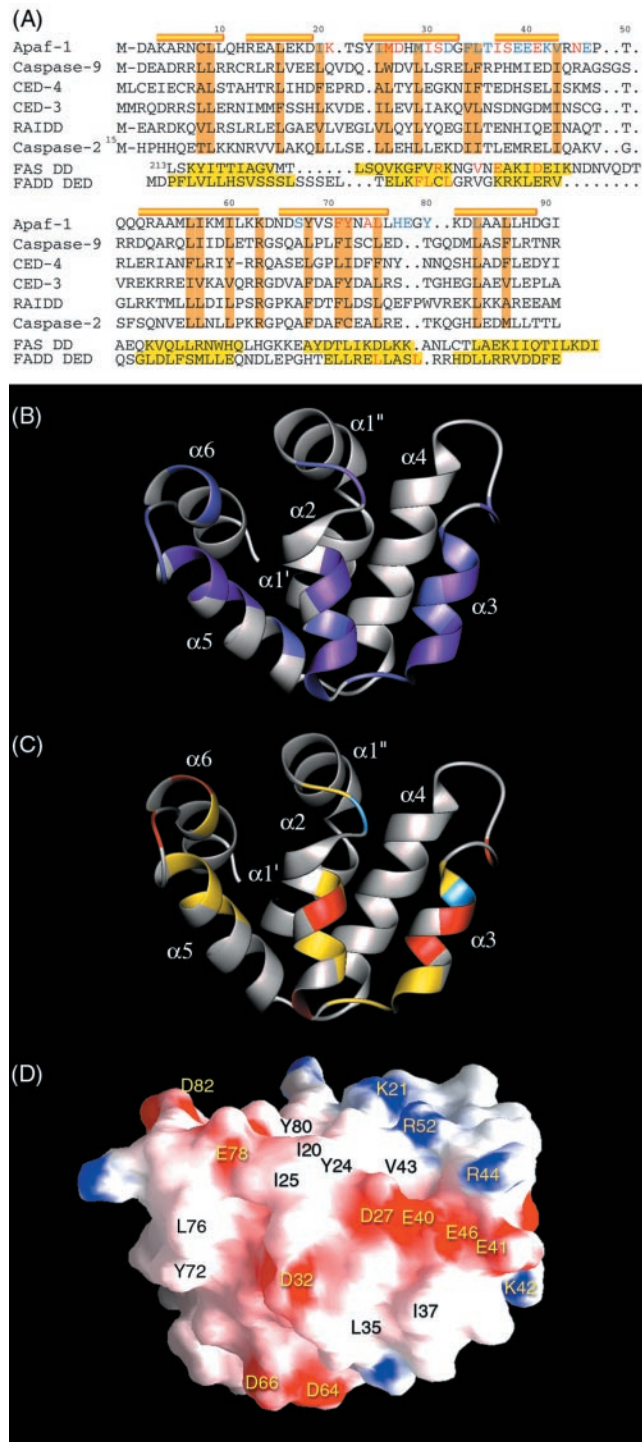FIG. 2.   Apaf-1 CARD binding surface is centered around α2 and α3. (*A*) Sequence alignment of the CARD members, Fas DD, and FADD DED. The α-helices identified in Apaf-1 CARD are represented by cylinders on top of the sequence alignment. Conserved hydrophobic residues are colored in brown. The chemically perturbed residues of Apaf-1 CARD observed during NMR titration experiments are divided into two groups. The residues showing severely broadened resonance during the titration are colored in red, whereas residues with shifted resonance are colored in blue. For Fas DD and FADD DED (20, 22), the helical regions are colored in yellow. In FAS DD, point mutations that disrupt the DD/DD homophilic interaction are colored in red. The proposed hydrophobic residues involved in FADD DED binding are also colored in red. (*B*) Ribbon diagram of Apaf-1 CARD highlighting the residues whose local chemical environments are perturbed during caspase-9 CARD binding. Residues of which NH resonance are severely broadened are colored in purple. Residues with shifted NH resonance are colored in light purple. (*C*)

extended to α5 (Fig. 2*B*). Among the three helices, α2 is the pivotal docking site. Interestingly, mutational studies on caspase-2 CARD suggest the involvement of D83 and E87 in the binding (23), both located on α5 according to the sequence alignment shown in Fig. 2*A*. The model of caspase-2 CARD, derived from the NMR structures of both Apaf-1 CARD and RAIDD CARD, also reveals an eminent acidic surface (Fig. 3*A*). Similar to that of Apaf-1 CARD, this surface is predominantly composed of acidic residues belonging to α2, α3, and α5. This suggests that Apaf-1 and caspase-2 CARDs function in similar fashions, both complementing the basic region of their corresponding binding partners. According to the previous studies on the CARD/CARD interaction between RAIDD and caspase-2 (21), the basic patch on RAIDD CARD consists of residue K6 and R10 of α1, R52, and R64 of α4. In agreement with this, caspase-9 CARD, which binds to Apaf-1 CARD, possesses a similar basic patch involving residues of α1 and α4 (R6, R7, R10, R11, R13, R15, R36, R52, R56, and R65). We thus propose that CARD/CARD homophilic interactions involve α2, α3, and α5 of one molecule and α1, α4 of the other. Interestingly, structural and mutagenesis studies on Fas DD indicate that α2 and α3 directly participate in binding (22). Similar studies on FADD DED also suggest the possible involvement of α2 and α3 in the homophilic interaction (20) (Fig. 2*A*).

Model of CARD/CARD Interaction Between Apaf-1 and Caspase-9. In the previous structural studies on RAIDD CARD and homology modeling of other CARD members (21), we propose, on the basis of the common existence of dipolar surface charge distribution in the CARD domains, that the formation of CARD/CARD complex is mediated by electrostatic interactions between the complementary charged surfaces. Knowing the structure and the binding surface of Apaf-1 CARD, we are able to construct a more elaborate model of CARD/CARD complex. On the basis of the sequence alignment presented in Fig. 2*A*, a model of caspase-9 CARD was constructed by using the atomic coordinates of Apaf-1 CARD. This modeling was performed by using the segment matching method (33). Clearly, a distinct basic surface encompassing residues R6, R7, R10, R11, R13, R15, R36, R52, R56, and R65 is observed in the modeled structure (Fig. 3 *A–C*). By using the general rule of electrostatic interactions between oppositely charged residues, we propose a model of the binary complex, which features the binding of α1 and α4 of caspase-9 CARD to the chemically perturbed surface (α2, α3, and α5) of Apaf-1 CARD. In this model, the largely acidic α2 and α3 of Apaf-1 CARD form a typical antiparallel four-helix bundle with the basic α1 and α4 of caspase-9 CARD. To further refine this interaction model, the orientations of the four helices are optimized according to the antiparallel four-helix bundles frequently observed in proteins (34) (Fig. 4*A*). In this model, the acidic residues of Apaf-1 including E39, E40, and E41 on α3, and D27 on α2 forms a contiguous acidic patch that interacts with the basic patch of caspase-9 CARD consisting of R6, R7, R10, R11, R13 on α1 and R52, R56 on α4. In addition to the charged residues, this model also shows direct interaction between the chemically perturbed and surface exposed hydrophobic residues of Apaf-1 (L35 and I37) and A46 of caspase-9. Other nearby hydrophobic residues, including I20, Y24, I25, and V43, can potentially contribute to

Ribbon diagram the same as in *B*. Here the chemically perturbed residues with hydrophobic, acidic, and basic sidechains are colored in yellow, red, and blue, respectively. (*D*) Surface diagram of Apaf-1 CARD in the same orientation as in *B* and *C*. In this figure, the surface electrostatic potential is color coded such that regions with electrostatic potentials $< -8\ k_{BT}$ are red, whereas those $> +8\ k_{BT}$ are blue (where k_B and T are the Boltzmann constant and temperature, respectively). Surface-exposed hydrophobic residues are labeled in black.
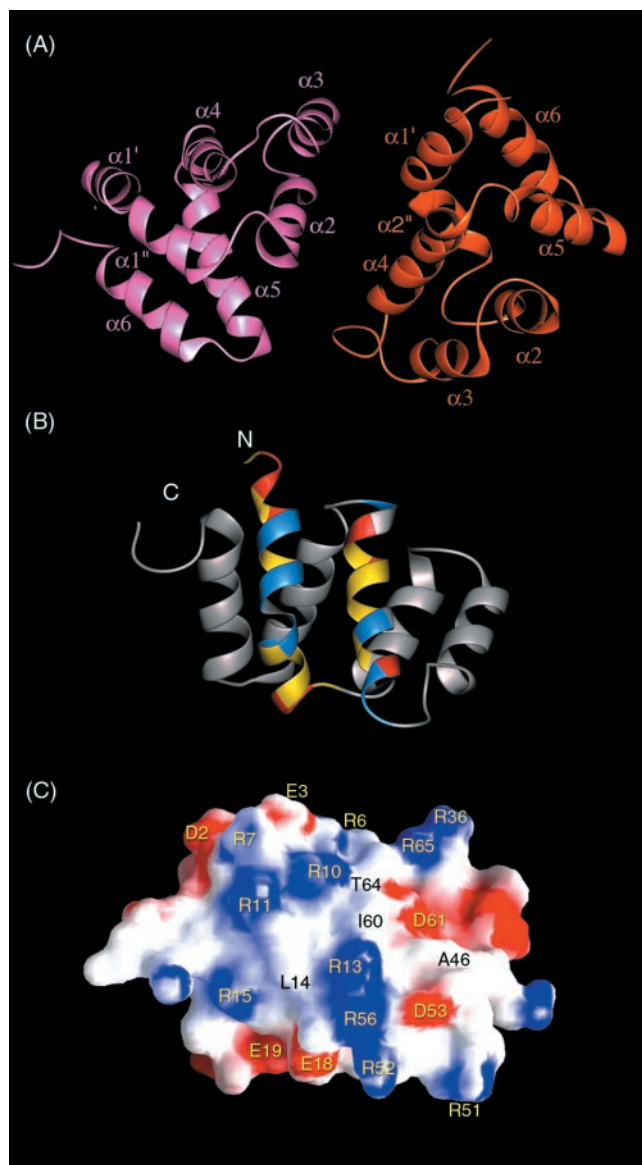
FIG. 3. Models of the Apaf-1/caspase-9 CARD complex. (*A*) Model of Apaf-1 CARD/caspase-9 CARD binary complex. Apaf-1 CARD is colored in pink, whereas caspase-9 CARD is colored in brown. The structure of caspase-9 CARD is constructed based on homology modeling of Apaf-1 CARD by using segment matching method (33). (*B*) Ribbon representation of caspase-9 CARD. The acidic, basic, and hydrophobic residues of $\alpha 1$ and $\alpha 4$ are colored in red, blue, and yellow, respectively. (*C*) Surface diagram of caspase-9 CARD in the same orientation as in *B*. In this figure, the surface electrostatic potential is color coded such that regions with electrostatic potentials $< -8\, k_{BT}$ are red, whereas those $> +8\, k_{BT}$ are blue (where k_B and T are the Boltzmann constant and temperature, respectively). Surface-exposed hydrophobic residues are labeled in black.

the binding energy via interactions with L14, I60, and T64 of caspase-9. In the Apaf-1 CARD of the modeled complex, $\alpha 5$ is farther away from the binding interface, although it seems to be an extension of the interaction surface defined by $\alpha 2$ and $\alpha 3$. However, several hydrophobic residues of $\alpha 5$ are also chemically perturbed. This suggests that there may exist a significant conformational change in the Apaf-1 CARD, which brings $\alpha 5$ to the interaction interface.

Specificity of the Homophilic Interactions. Apaf-1 CARD, FADD DED, and Fas DD are structurally similar, and all interact with their partners through the surface defined by $\alpha 2$ and $\alpha 3$. However, there are stringent selectivities among the three families of recruitment domains that define their roles in
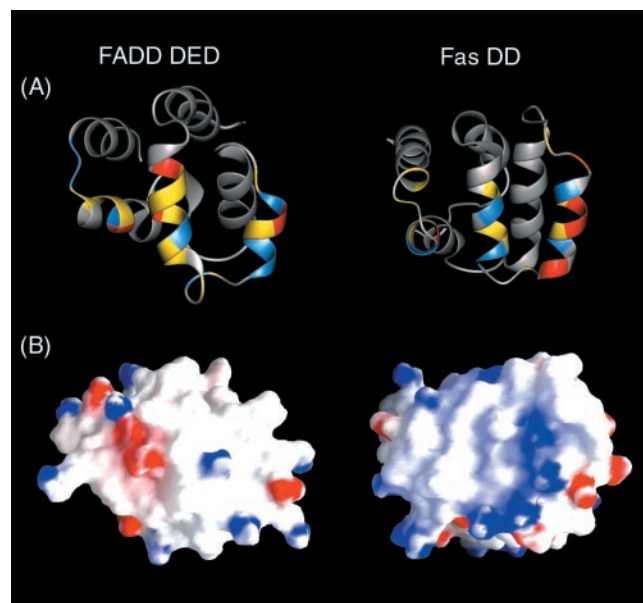

FIG. 4. Surface properties of FADD DED and Fas DD containing $\alpha 2$, $\alpha 3$, and $\alpha 5$. (*A*) Ribbon representation of FADD DED and Fas DD. The acidic, basic, and hydrophobic residues of $\alpha 2$, $\alpha 3$, and $\alpha 5$ are colored in red, blue, and yellow, respectively. (*B*) Surface diagram of FADD DED and Fas DD in the same orientations as in *A*. In this figure, the surface electrostatic potential is color coded such that regions with electrostatic potentials $< -8\, k_{BT}$ are red, whereas those $> +8\, k_{BT}$ are blue (where k_B and T are the Boltzmann constant and temperature, respectively).

various apoptotic signaling pathways. It is interesting to know what features render procaspase-9 capable of being recruited by Apaf-1 CARD and not by FADD DED or Fas DD. A comparison of surface properties of FADD DED, Fas DD, and Apaf-1 CARD gives a possible explanation. Among the three domains, the most significant difference lies in $\alpha 2$ and $\alpha 3$. For Apaf-1 CARD, the surface of $\alpha 2$ and $\alpha 3$ is primarily acidic, whereas the similar surface is basic in Fas DD. The corresponding surface of FADD DED shows only a smaller basic patch compared with Fas DD. These differences may introduce conflicts that eliminate the possibility of caspase-9 recruitment by FADD DED and Fas DD associated with the Fas/tumor necrosis factor pathway.

CONCLUSIONS

We have determined the solution structure of Apaf-1 CARD using NMR spectroscopy. The structure resembles the six-helix bundle fold observed in other homophilic interaction motifs involved in apoptotic pathways, including RAIDD CARD, FADD DED, and FAS DD. A unique feature of Apaf-1 CARD is that there exists a kink of approximately 50° in the middle of $\alpha 1$, which breaks the helix into two shorter helices ($\alpha 1'$ and $\alpha 1''$). On the basis of the results from NMR experiments that monitor the chemical perturbations of Apaf-1 CARD being titrated with caspase-9 CARD, we have identified the surface region of Apaf-1 CARD, encompassing $\alpha 2$, $\alpha 3$, and $\alpha 5$, as the binding surface. This interaction surface is primarily acidic. However, it also contains a significant number of hydrophobic residues that are chemically perturbed. By docking the basic surface ($\alpha 1$ and $\alpha 4$) of caspase-9 CARD onto the acidic surface ($\alpha 2$, $\alpha 3$, and $\alpha 5$) of Apaf-1 CARD, in combination with analyses of the homophilic interaction between RAIDD and caspase-2 CARD, we constructed a general model of CARD/CARD complexes. In this model, $\alpha 2$, $\alpha 3$, and $\alpha 5$ of one CARD interact with $\alpha 1$ and $\alpha 4$ of the other CARD. Furthermore, the interface highlights the packing of

Apaf-1 $\alpha2/\alpha3$ and caspase-9 $\alpha1/\alpha4$ into an antiparallel four-helix bundle. Interestingly, we observed chemical perturbation for a large portion of residues of $\alpha5$, a helix in Apaf-1 CARD that is slightly tilted away from the binding interface. We believe that there may be a binding-induced conformational change in Apaf-1 CARD that can bring this helix to the proximity of the interaction site.

During the final stage of preparation of this manuscript, Qin *et al.* reported the crystal structure of the CARD/CARD complex between Apaf-1 and procaspase-9 (36). In their studies, both mutagenesis and structural data conform to the general mode of electrostatic interactions shown here and proposed previously (21). For the most part, the binding interface revealed by the crystal structure is consistent with our NMR studies. Nevertheless, chemical shift perturbation data recorded in solution indicate that there may exist a change of the relative orientation of $\alpha2$, $\alpha5$, and $\alpha6$ during the assembly of the CARD/CARD complex (Fig. 2 *B* and *C*).

1. Thompson, C. B. (1995) *Science* **267,** 1456–1462.
2. Green, D. R. (1998) *Cell* **94,** 695–698.
3. Green, D. R. & Reed, J. C. (1998) *Science* **281,** 1309–1312.
4. Nagata, S. (1997) *Cell* **88,** 355–365.
5. Boldin, M. P., Goncharov, T. M., Goltsev, Y. V. & Wallach, D. (1996) *Cell* **85,** 803–815.
6. Muzio, M., Chinnaiyan, A. M., Kischkel, F. C., O'Rourke, K., Shevchenko, A., Ni, J., Scaffidi, C., Bretz, J. D., Zhang, M., Gentz, R., *et al.* (1996) *Cell* **85,** 817–827.
7. Yang, X., Chang, H. Y. & Baltimore, D. (1998) *Mol. Cell* **1,** 319–325.
8. Zou, H., Henzel, W. J., Liu, X., Lutschg, A. & Wang, X. (1997) *Cell* **90,** 405–413.
9. Zou, H., Li, Y., Liu., X. & Wang, X. (1999) *J. Biol. Chem.* **274,** 11549–11556.
10. Srinivasula, S. M., Ahmad, M., Fernandes-Alnemri, T. & Alnemri, E. S. (1998) *Mol. Cell* **1,** 949–957.
11. Cecconi, F., Alvarez-Bolado, G., Meyer, B. I., Roth, K. A. & Gruss, P. (1998) *Cell* **94,** 727–737.
12. Hakem, R., Hakem, A., Duncan, G. S., Henderson, J. T., Woo, M., Soengas, M. S., Elia, A., de la Pompa, J. L., Kagi, D., Khoo, W., *et al.* (1998) *Cell* **94,** 339–352.
13. Kuida, K., Haydar, T. F., Kuan, C. Y., Gu, Y., Taya, C., Karasuyama, H., Su, M. S., Rakic, P. & Flavell, R. A. (1998) *Cell* **94,** 325–337.
14. Yoshida, H., Kong, Y. Y., Yoshida, R., Elia, A. J., Hakem, A., Hakem, R., Penninger, J. M. & Mak, T. W. (1998) *Cell* **94,** 739–750.
15. Soengas, M. S., Alarcon, R. M., Yoshida, H., Giaccia, A. J., Hakem, R., Mak, T. W. & Lowe, S. W. (1999) *Science* **284,** 156–159.
16. Li, H., Zhu, H., Xu, C. J. & Yuan, J. (1998) *Cell* **94,** 491–501.
17. Luo, X., Budihardjo, I., Zou, H., Slaughter, C. & Wang, X. (1998) *Cell* **94,** 481–490.
18. Kuwana, T., Smith, J. J., Muzio, M., Dixit, V., Newmeyer, D. D. & Kornbluth, S. (1998) *J. Biol. Chem.* **273,** 16589–16594.
19. Hofmann, K., Bucher, P. & Tschopp, J. (1997) *Trends Biochem. Sci.* **22,** 155–156.
20. Eberstadt, M., Huang, B., Chen, Z., Meadows, R. P., Ng, S. C., Zheng, L., Lenardo, M. J. & Fesik, S. W. (1998) *Nature (London)* **392,** 941–945.
21. Chou, J. J., Matsuo, H., Duan, H. & Wagner, G. (1998) *Cell* **94,** 171–180.
22. Huang, B., Eberstadt, M., Olejniczak, E. T., Meadows, R. P. & Fesik, S. W. (1996) *Nature (London)* **384,** 638–641.
23. Duan, H. & Dixit, V. M. (1997) *Nature (London)* **385,** 86–89.
24. Clore, G. M. & Gronenborn, A. M. (1994) *Methods Enzymol.* **239,** 349–363.
25. YamaZaki, T., Lee, W., Arrowsmith, C. H., Muhandiram, D. R. & Kay, L. E. (1994) *J. Am. Chem. Soc.* **116,** 11655–11666.
26. Matsuo, H., Li, H., MCGuire, A. B., Fletcher, C. M., Gingras, A., Sonenberg, N. & Wagner, G. (1997) *Nat. Struct. Biol.* **4,** 717–724.
27. Szypserski, T., Neri, D., Leiting, B., Otting, G. & Wuthrich, K. (1992) *J. Biomol. NMR* **2,** 323–334.
28. Bax, A., Griffey, R. H. & Hawkins, B. L. (1983) *J. Magn. Reson.* **55,** 301–315.
29. Güntert, P., Mumenthaler, C. & Wüthrich, K. (1997) *J. Mol. Biol.* **273,** 283–298.
30. Wishart, D. S. & Sykes, B. D. (1994) *J. Biomol. NMR* **4,** 171–180.
31. Brünger, A. T. (1994) in *x-plor Manual 3.851: A System for X-Ray Crystallography and NMR.* X-PLOR Version 3.851 (Yale Univ. Press, New Haven, CT).
32. Sun, Z. J., Dötsch, V., Kim, M., Li, J., Reinhez, E. L. & Wagner, G. (1999) *EMBO J.* **18,** 2941–2949.
33. Levitt. M. (1992) *J. Mol. Biol.* **226,** 507–523.
34. Branden, C. and Tooze, J. (1991) in *Introduction to Protein Structure* (Garland, New York), pp. 33–41.
35. Laskowski, R. A., MacArthur, M. W., Moss, D. S. & Thornton, J. M. (1993) *J. Appl. Crystallogr.* **26,** 283–291.
36. Qin, H., Srinivasula, S. M., Wu, G., Fernandes-Alnemri, T., Alnemri, E. S. & Shi., Y. (1999) *Nature (London)* **399,** 549–557.